

Comparison of primary aerosol emission and secondary aerosol formation from gasoline direct injection and port fuel injection vehicles

Zhuofei Du¹, Min Hu^{1,3*}, Jianfei Peng^{1†}, Wenbin Zhang², Jing Zheng¹, Fangting Gu¹, Yanhong Qin¹, Yudong Yang¹, Mengren Li¹, Yusheng Wu¹, Min Shao¹, Shijin Shuai²

1. State Key Joint Laboratory of Environmental Simulation and Pollution Control, College of Environmental Sciences and Engineering, Peking University, Beijing 100871, China

2. State Key Laboratory of Automotive Safety and Energy, Department of Automotive Engineering, Tsinghua University, Beijing 100084, China

3. Beijing Innovation Center for Engineering Sciences and Advanced Technology, Peking University, Beijing 100871, China

[†] Now at Department of Atmospheric Sciences, Texas A&M University, College Station, TX 77843, US

*Corresponding author: Min Hu, minhu@pku.edu.cn

Abstract

Gasoline vehicles significantly contribute to urban particulate matter (PM) pollution. Gasoline direct injection (GDI) engines, known as their higher fuel efficiency than that of port fuel injection (PFI) engines, have been increasingly employed in new gasoline vehicles. However, the impact of this trend on air quality is still poorly understood. Here, we investigated both primary emissions and secondary organic aerosol (SOA) formation from a GDI and a PFI vehicle under an urban-like driving condition, using combined approaches involving chassis dynamometer measurement and environmental chamber simulation. The PFI vehicle emits slightly more volatile organic compounds, e.g., benzene and toluene, whereas the GDI vehicle emits more particulate components, e.g., the total PM, elemental carbon, primary organic aerosols and polycyclic aromatic hydrocarbons. Strikingly, we found a much higher SOA production (by a factor of approximately 2.7) from the exhaust of the GDI vehicle than that of

the PFI vehicle under the same conditions. More importantly, the higher SOA production found in the GDI vehicle exhaust occurs concurrently with lower concentrations of traditional SOA precursors, e.g., benzene and toluene, indicating a greater contribution of intermediate volatility organic compounds and semivolatile organic compounds in the GDI vehicle exhaust to the SOA formation. Our results highlight the considerable potential contribution of GDI vehicles to urban air pollution in the future.

1 Introduction

Organic aerosols (OAs) account for approximately 20-50 % of ambient fine particulate matter ($PM_{2.5}$), with significant environment, climate and health effects (Maria et al., 2004; Kanakidou et al., 2005). Primary organic aerosol (POA) is emitted directly by sources, while secondary organic aerosol (SOA) is mainly formed via oxidation of gaseous precursors in the atmosphere and account for about 30-90 % of the OA mass worldwide (Zhang et al., 2007; Hu et al., 2016), but SOA source remain poorly constrained. Robinson et al. (2007) proposed that low-volatility gas-phase species emitted from diesel vehicles were important sources for urban ambient SOA, which achieved better mass closure between observed and modeled SOA. Using an updated CMAQ model, Jathar et al. (2017) found that 30-40% OA was contributed from vehicles in the southern California, and half of which was SOA. Huang et al. (2014) recently revealed that 15-65 % of SOA was contributed by fossil fuel consumption (i.e., traffic and coal burning) in megacities in China. Zhao et al. (2016) also reported that intermediate volatility organic compounds (IVOCs) from vehicles constituted a large percentage of SOA concentration in China by chamber experiments as well as the two-dimensional volatility basis set (2D-VBS) box model simulations. These findings indicated that vehicles have important contribution to ambient SOA in urban areas. An ambient organic aerosol measurement in the Los Angeles Basin demonstrated that SOA contributed from gasoline vehicles was significant in the urban air, much larger than that from diesel vehicles (Bahreini et al., 2012). A similar conclusion was reached by Hayes et al. (2013) based on mass spectrometer results. Meanwhile, several chamber simulation studies concluded that the exhaust of gasoline vehicles could form substantial SOA (Jathar et al., 2014). Thus,

51 gasoline vehicle exhaust is highly associated with ambient SOA formation.

52 Gasoline vehicles can be categorized into two types based on the fuel injection technologies in their engines,
53 i.e., port fuel injection (PFI) vehicles and gasoline direct injection (GDI) vehicles. Unlike a PFI engine, in which
54 gasoline is injected into intake port, gasoline is sprayed into cylinder directly in a GDI engine. With the increased
55 atomization and vaporization rate of fuel, and more accurate control of fuel volume and injection time, a GDI
56 engine has many advantages, such as better fuel efficiency, lower CO₂ emissions and less fuel pumping loss
57 (Alkidas, 2007; Myung et al., 2012; Liang et al., 2013). In past decades, PFI vehicles dominated the market share
58 of gasoline cars in the world. However, in recent years, GDI vehicles have been increasingly employed, due to their
59 higher fuel efficiency. The market share of GDI vehicles in sales in 2016 reached about 25 %, 50 % and 60 % in
60 China, the US and Europe, respectively (Wen et al., 2016; Zimmerman et al., 2016).

61 Several previous studies investigated the emissions of GDI and PFI vehicles, in terms of concentrations of
62 gaseous pollutants, particle numbers and mass concentrations, and evaluated the reduction of emissions with
63 upgrading emission standards (Ueberall et al., 2015; Zhu et al., 2016; Saliba et al., 2017). These studies showed
64 that GDI vehicles emitted more primary particles than PFI vehicles (Zhu et al., 2016; Saliba et al., 2017), and even
65 diesel vehicles equipped with a diesel particulate filter (DPF) (Wang et al., 2016). These higher primary particle
66 emissions are likely due to insufficient time allowed for gasoline fuel to be mixed with air thoroughly, as well as
67 gasoline droplets impinging onto pistons and surfaces of combustion chamber in GDI engine (Chen et al., 2017;
68 Fu et al., 2017). However, in most studies, vehicles were tested under the driving cycles of the US or European
69 standards; those results may not representative of China's traffic conditions.

70 SOA production from gasoline vehicle exhaust was previously simulated in smog chambers and potential
71 aerosol mass (PAM) flow reactors. SOA formed from gaseous pollutants exceeds the related POA emissions and
72 has much more contribution to air quality degradation. These studies mostly focused on the impacts of SOA
73 formation by the model year (Gordon et al., 2014; Jathar et al., 2014; Liu et al., 2015), fuel formulations (Peng et
74 al., 2017), driving cycles (including idling) (Nordin et al., 2013; Platt et al., 2013) and start-up modes of the gasoline
75 vehicles (Nordin et al., 2013). Few studies, however, have investigated SOA formation from vehicles with different

76 engine technologies (GDI and PFI) under the same working condition.

77 In this study, both primary emissions and secondary aerosol formation from GDI and PFI vehicles were
78 investigated. To represent typical urban driving patterns in megacities such as Beijing, the tested vehicles used
79 gasoline fuel meeting the China Phase V fuel standard, and were operated over the cold-start Beijing cycle (BJC).
80 The SOA formation from both the PFI and GDI vehicle exhausts were then simulated using a smog chamber.
81 Finally, the overall contributions of the GDI and PFI gasoline vehicles to ambient particulate matter (PM) were
82 evaluated. This study is part of a project that investigates the relationship between vehicle (engine) emissions and
83 ambient aerosols, including potential of SOA formation from a PFI engine (Du et al., 2017) and the effects of
84 gasoline aromatics on SOA formation (Peng et al., 2017).

85

86 **2 Materials and methods**

87 **2.1 Vehicles**

88 One PFI vehicle and one GDI vehicle were tested in this study to investigate their primary emissions and SOA
89 formation. The vehicles were certified to the China Phase IV Emissions Standard (equivalent to Euro IV) and the
90 China Phase V Emissions Standard (equivalent to Euro V), respectively. More information of the vehicles is shown
91 in Table 1. The fuel used in the experiments was a typical Phase V gasoline on the China market (sulfur content =
92 6 mg kg⁻¹). More information on the fuel is provided in Table S1 in the Supplement. Cold-start BJC, characterized
93 by a higher proportion of idling periods and lower acceleration speeds than the New European Driving Cycle
94 (NEDC), was performed to simulate the repeated braking and acceleration on road in megacities such as Beijing.
95 The BJC lasted for approximately 17 minutes, with a maximum speed of 50 km h⁻¹ (Peng et al., 2017).

96

97 **2.2 Experimental setup**

98 The chamber experiments were carried out in the summer at the State Key Laboratory of Automotive Safety
99 and Energy of Tsinghua University in Beijing, including two experiments conducted with the GDI vehicle and four
100 experiments conducted with the PFI vehicle. The tested vehicles were placed on a chassis dynamometer system

(Burke E. Porter Machinery Company) with a controlled room temperature of 26.4 ± 2.5 °C and absolute humidity of 11.5 ± 2.4 g m⁻³. The exhaust emitted by the vehicle tailpipe was diluted in a constant volume sampler (CVS) system, where the flowrate was maintained at 5.5 m³ min⁻¹ using filtered ambient air, achieving about 20-fold dilution of the exhaust. Several instruments, including an AVL CEBII gas analyzer, a Combustion Differential Mobility Spectrometer (DMS500) and a particle sampler, were connected to the CVS (detailed in Figure 1 and section 2.3) to characterize the primary gas- and particulate-phase pollutants. The diluted exhaust produced by the CVS system was injected into an outdoor chamber, where secondary aerosol formation was simulated. This was the second dilution step of the exhaust with a dilution factor of approximately 15. A schematic illustration of the outdoor experimental setup is shown in Figure 1.

The photochemical oxidation experiments were carried out in a quasi-atmospheric aerosol evolution study (QUALITY) outdoor chamber. More details of the setup and performance of the QUALITY chamber were introduced by Peng et al. (2017). Prior to each experiment, the chamber was covered with a double-layer anti-ultraviolet (anti-UV) shade to block sunlight and was cleaned with zero air for about 15 h to create a clean environment. Approximately 120 ppb O₃ were injected into the chamber prior to the injection of the vehicle exhaust to make the oxidation environment similar to the mean O₃ peak concentration in the ambient atmosphere. Before the chamber was exposed to sunlight, about 15-minute period was left to ensure that the pollutants were mixed sufficiently in the chamber, then the initial concentrations were characterized in the dark. Subsequently, the anti-UV shade was removed from the chamber and photo-oxidation was initiated. A suite of high time resolution instruments was utilized to track the evolution of pollutants during the chamber experiments. Zero air was added into the chamber during sampling period to maintain a constant pressure.

121

122 2.3 Instrumentation

Primary gases and aerosols were measured by the instruments connected to the CVS. The concentrations of gaseous pollutants, including CO, CO₂, NO_x and total hydrocarbon (THC) were monitored with a gas analyzer AVL Combustion Emissions Bench II (CEB II, AVL, Austria). Primary aerosols were measured with both on-line

126 and off-line instruments. A DMS500 (Cambustion, UK) was implemented to monitor the real-time number size
127 distribution and total number concentration of primary particles. Its sampling line was heated to maintain the
128 temperature at 150°C. The aerosols were also collected on Teflon and quartz filters by AVL Particulate Sampling
129 System (SPC472, AVL, Austria) to analyze the mass, organic carbon (OC) and elemental carbon (EC) emission
130 factors using a balance and an OC/EC analyzer (Sunset Lab, USA).

131 During the chamber experiments, a suite of real-time instruments was utilized to characterize the evolution of
132 the gas and particulate-phase pollutants. A CO analyzer, a NO-NO₂-NO_x analyzer and an O₃ analyzer (Thermo
133 Fisher Scientific Inc., USA) were employed to measure the concentrations of CO, NO_x (including NO and NO₂)
134 and O₃, respectively. The evolution of volatile organic compounds (VOCs) was monitored with a proton transfer
135 reaction mass spectrometer (PTR-MS, IoniconAnalytik, Austria) (Lindinger et al., 1998). H₃O⁺ was used as the
136 reagent ion, which reacted with the target compounds. The resulting ions were detected by a quadrupole mass
137 spectrometer. Meanwhile, the particles size distribution was characterized using a scanning mobility particle sizer
138 system (SMPS, TSI, USA), which consisted of a differential mobility analyzer (DMA, TSI, USA) and a
139 condensation particle counter (CPC, TSI, USA). This system can measure aerosols with diameters ranging from 15
140 nm to 700 nm. A high-resolution time-of-flight aerosol mass spectrometer (HR-ToF-AMS, Aerodyne Research,
141 USA) was used to obtain mass concentrations and size distributions of submicron, non-refractory aerosols,
142 including sulfate, nitrate, ammonium, chloride and organic (DeCarlo et al., 2006). Table 2 lists the instruments used
143 to measure the primary emissions and their evolutions in the chamber experiments.

144

145 **3 Results**

146 **3.1 Primary emissions**

147 **Gaseous pollutant emissions**

148 Emission factors (EFs) of CO₂, THC, benzene and toluene from the GDI and PFI vehicles are listed in Table
149 3. The EFs of CO₂ and THC are derived from measured concentrations in CVS, while the EFs of benzene and
150 toluene were calculated from the initial concentrations in the chamber. The THC emission factor was reported in

151 units of carbon mass, $\text{g C kg}^{-1}\text{fuel}^{-1}$.

152 The GDI vehicle emitted less CO_2 and THC than the PFI vehicle due to their different fuel injection strategies
153 and mixing features (Liang et al. 2013; Gao et al., 2015). The EF of THC from the GDI vehicle met the standard
154 of the China Phase V Emission Standard (0.1 g km^{-1}), but that from the PFI vehicle was slightly above the standard
155 limit. The PFI vehicle used in this study met a less stringent emission standard (the China Phase IV), which might
156 cause additional THC emissions when compared to the China Phase V Emission Standard. In addition, in this study
157 we employed the BJC whereas the standard is based on the NEDC. More repeated braking and acceleration in the
158 BJC (Figure S2) might cause incomplete combustion and consequently higher THC emission from the PFI vehicle.
159 As typical VOC species emitted by vehicles, benzene and toluene were measured in this study. For both vehicles,
160 the EFs of toluene were higher than those of benzene. Consistent with the feature of THC emission, the PFI vehicle
161 emitted more benzene and toluene than the GDI vehicle, and the enhancement of toluene was much larger than that
162 of benzene.

163 The EFs of the gaseous pollutants in this study had similar magnitudes to those in previous studies in which
164 gasoline vehicles met comparable levels of emission standards and were tested under cold-start driving condition,
165 while the results in this study were slightly higher, as shown in Table 3. This difference might be because the
166 California ultralow-emission vehicles (ULEV) (Saliba et al., 2017) and most LEV II vehicles (manufactured in
167 2004 or later) (May et al., 2014) meet the US certification gasoline emission standards for the ULEV category,
168 which has a lower limit of gaseous pollutants than the China Phase V Emission Standard. In addition, the different
169 driving cycles of our study from those other studies (listed in Table 3) might be another explanation for the
170 difference in the EFs of gaseous pollutants.

171 **Primary particle emissions**

172 The EFs of PM, elemental carbon (EC), POA and particulate polycyclic aromatic hydrocarbons (PAHs) are
173 shown in Table 4. The EF of $\text{PM}_{2.5}$ from the GDI vehicle was about 1.4 times higher than that of the PFI vehicle.
174 Both vehicles met the China Phase V Emission Standard for PM emission (4.5 mg km^{-1}). The GDI vehicle emitted
175 about 3.3 times more EC and 1.2 times more POA than the PFI vehicle. The primary carbonaceous aerosols

(EC+POA) accounted for 85 % and 82 % of the PM in the GDI and PFI vehicles respectively, suggesting that carbonaceous aerosols were the major components in the PM from gasoline vehicles, especially for the GDI vehicle.

PAHs account for a small fraction of particulate organic matter in the atmosphere, but the molecular signature of PAHs can be utilized in source identification of vehicle emissions (Kamal et al., 2015). The GDI vehicle emitted about 1.5 times the PAHs of the PFI vehicle. The EFs of PAH compounds are listed in Table S2 in the Supplement, and the details of PAHs measurement were described in Li et al. (2016). It should be noted that the PAHs were tested under warm-start cycles. A higher EF of PAHs would be obtained under a cold-start cycle, since the lower temperature would lead to inefficient catalyst at the beginning of cold-start (Mathis et al., 2005). The main contributors to the total PAH mass emitted from gasoline vehicle exhaust in this study, especially from the GDI vehicle exhaust, were similar with the results reported by previous studies (Schauer et al., 2002; Hays et al., 2013).

The lower PM_{2.5} and POA emissions from GDI vehicle were found in previous studies, except that a little higher PM_{2.5} emission from GDI vehicle was illustrated in Saliba's study (Platt et al., 2013; May et al., 2014; Zhu et al., 2016; Saliba et al., 2017). The EC emissions were in the range of those of previous studies but on the lower level. The EF of the POA measured in this study was higher than those of other studies, leading to a higher OC/EC ratio, which could be attributed to the less strict emission standard of our vehicles and the different driving cycles applied in the experiments.

The bimodal number size distributions of the primary PM from the vehicles measured by the DMS500 are shown in Figure 2. The particle distributions of the exhaust of the GDI and PFI vehicles illustrated similar patterns, with two peaks located at about 10 nm for nucleation mode and at 60-90 nm for accumulation mode, respectively, which are consistent with the results of previous studies (Maricq et al., 1999; Chen et al., 2017). The particle number size distribution of the exhaust of the GDI vehicle showed a similar pattern to that of the PFI vehicle, with a much higher number concentration that is consistent with the emission of more particle mass.

3.2 SOA formation from gasoline vehicle exhaust

The time-resolved concentrations of gases and particles during the chamber experiments are illustrated in

Figure 3. Before removing the anti-UV shade, the initial concentrations of NO_x, benzene and toluene from the PFI and GDI vehicles were 80 ppb, 3 ppb, 5 ppb and 100 ppb, 4 ppb, 14 ppb respectively.

After the aging experiment started (t=0 in Figure 3), NO was formed from NO₂ photolysis, and then reacted with O₃ to form NO₂. The O₃ concentration increased rapidly to a maximum within 2-3 h and then decreased via reactions and dilution. Benzene and toluene decayed at different rates during the aging process.

New particle formation was found inside the chamber 15 minutes after the exhaust was exposed to sunlight, providing substantial seeds for secondary aerosol formation. Significant growth of particles in both size and mass was observed in the chamber, indicating that a large amount of secondary aerosol was formed during the photochemical oxidation. The chemical composition of the secondary aerosols was measured continuously by a HR-ToF-AMS. Organic was the dominant composition of the secondary aerosol, accounting for 88-95 % of the total particle mass inside the chamber (Figure S1), which is consistent with our previous research (Peng et al., 2017). The SOA mass exhibited different growth rate for the two types of vehicles. After a 4 h oxidation in the chamber, the SOA formed from the exhaust of the GDI vehicle was approximately double that of the PFI vehicle.

The solar radiation conditions significantly influenced the SOA formation. Thus, OH exposure was used to characterize the photochemical age as a normalization, instead of the experiment time. Two VOC species with noticeable differences in their reaction rate constants with OH radicals could be utilized to calculate the OH exposure ([OH] Δt) based on Equation 1 (for benzene and toluene, as used in this study) (Yuan et al., 2012).

$$[\text{OH}] \Delta t = \frac{1}{k_T - k_B} \times \left(\ln \frac{[T]}{[B]} \Big|_{t=0} - \ln \frac{[T]}{[B]} \right) \quad (1)$$

where k_T and k_B are the OH rate constants of benzene ($1.2 \times 10^{-12} \text{ cm}^3 \text{ molecule}^{-1} \text{ s}^{-1}$) (Yuan et al., 2012) and toluene ($5.5 \times 10^{-12} \text{ cm}^3 \text{ molecule}^{-1} \text{ s}^{-1}$) (Kramp and Paulson, 1998), respectively. $\frac{[T]}{[B]} \Big|_{t=0}$ is the concentration ratio of toluene to benzene at the beginning of the aging process, and $\frac{[T]}{[B]}$ is their concentration ratio measured during aging process.

The SOA concentrations as a function of OH exposure are illustrated in Figure 4. Wall-loss correction and dilution correction, including both particles and gaseous pollutants, were taken into consideration in the calculation

225 of the SOA mass concentration in the chamber. Detailed descriptions of corrections are given in the Supplement.
226 Assuming the mean OH concentration was 1.6×10^6 molecular cm^{-3} in Beijing (Lu et al., 2013), the whole aging
227 procedure in the chamber experiments was equal to a 6-10 h atmospheric photochemical oxidation. The average
228 SOA concentrations were 9.25 ± 1.80 and 4.68 ± 1.32 $\mu\text{g m}^{-3}$ for the GDI and PFI vehicles, respectively, when the
229 OH exposure was 5×10^6 molecular cm^{-3} h in the chamber. Considering the driving cycle mileage and fuel
230 consumption, the SOA productions were 54.77 ± 10.70 $\text{mg kg}^{-1}_{\text{fuel}}$ or 3.06 ± 0.60 mg km^{-1} for the GDI vehicle and
231 20.57 ± 5.82 $\text{mg kg}^{-1}_{\text{fuel}}$ or 1.55 ± 0.44 mg km^{-1} for the PFI vehicle. Compared with the PFI vehicle, the GDI vehicle
232 exhaust exhibited a higher potential of SOA formation, even though the PFI vehicle emitted more VOCs, which
233 are considered as dominant classes of SOA precursors. This result indicates that higher concentrations of some
234 other SOA precursors exist in the exhaust of GDI vehicles, which will be further discussed in section 3.3.

235 The results from chamber simulation of SOA formation from individual gasoline vehicles are illustrated in
236 Figure 5. The SOA production from the both vehicles in this study is in the range of the results of previous studies
237 (Nordin et al., 2013; Platt et al., 2013; Jathar et al., 2014; Liu et al., 2015; Peng et al., 2017). The variation of the
238 SOA production among these studies might be caused by several factors: the model years of vehicles
239 (corresponding to emission standards) (Nordin et al., 2013; Liu et al., 2015), their driving cycles (Nordin et al.,
240 2013), the initial concentrations of gaseous pollutants in the chamber (Jathar et al., 2014), and the ratio of VOCs to
241 NO_x (Zhao et al., 2017) in the chamber experiments.

242 To investigate the dominant contributors to ambient PM from the GDI and PFI vehicles, Figure 6 illustrates
243 the EFs of EC and POA as well as the production factors of SOA in this study. The SOA production from the GDI
244 vehicle was approximately 2.7 times higher than that from the PFI vehicle. At 5×10^6 molecular cm^{-3} h OH exposure,
245 the SOA/POA ratio was close to unity. Figure 4 illustrates that the SOA production increased with photochemical
246 age rapidly (within 2×10^7 molecular cm^{-3} h). Thus, SOA would exceed POA at higher OH exposure, e.g., the
247 SOA/POA ratio reached about 4 at 10^7 molecular cm^{-3} h OH exposure, becoming the major PM contributor. In
248 terms of the POA and EC emissions as well as the SOA formation, the GDI vehicle contributed 2.2 times more
249 than the PFI vehicle.

Although particle wall-loss correction as well as particle and gas dilution corrections were considered in this study, several factors may still contribute to the uncertainties of the SOA production. First, the loss of semi-volatile vapors to the chamber walls was not corrected, which may result in an underestimation of the rate of SOA production with a factor of 1.1-4.1 (Zhang et al., 2014). Second, under some ambient conditions such as severe urban haze events (Guo et al., 2014), particle mass concentrations can be as high as 200-300 $\mu\text{g m}^{-3}$, much higher than the $23 \pm 6 \mu\text{g m}^{-3}$ under the chamber conditions of this study. High particle mass loadings are favorable for the partitioning of semi-volatile compounds into the particle phase, potentially increasing SOA mass yields (Odum et al., 1996; Donahue et al., 2006). Third, stronger partitioning of SOA precursors into the particle phase may reduce oxidation rate in the gas phase, which will potentially reduce the rate of SOA production (Seinfeld et al., 2003; Donahue et al., 2006).

3.3 SOA mass closure

SOA production ($\Delta\text{OA}_{\text{predicted}}$) estimated from VOC precursors can be defined as Eq. (2):

$$\Delta\text{OA}_{\text{predicted}} = \sum_i (\Delta_i \times Y_i) \quad (2)$$

where Δ_i is the concentration change of precursor VOC_i measured with PTR-MS in the chamber experiments, and Y_i is the SOA yield of the VOC_i . In this study, benzene, toluene, C8 alkylbenzene (e.g., ethylbenzene and o-, m-, p-xylene) and C9 alkylbenzene (e.g., n-, i-propylbenzene, o-, m-, p-ethyltoluene, and 1,2,3-, 1,2,4-, 1,3,5-trimethylbenzene) were involved in the estimation of SOA production, and alkanes and alkenes were not considered. A recent study found that ozonolysis of alkenes from gasoline vehicle exhaust could form SOA through aldol condensation reactions (Yang et al., 2018). However, much low declines of concentrations were observed than those of aromatics during chamber experiments, so alkenes might not play significant role in SOA formation in this study.

The SOA yield is sensitive to the VOCs/NO_x ratio (Song et al., 2005). In this study, the VOCs/NO_x ratio was in the range of 0.5-1.0 ppbC/ppb, thus, the SOA formation from the vehicle exhaust was determined under high NO_x conditions. The high NO_x SOA yields of benzene and toluene were taken from Ng et al. (2007). The C8 and

C9 alkylbenzenes used the SOA yield of m-xylene from Platt et al. (2013).

The increased predicted SOA contribution from the VOC precursors as a function of OH exposure accumulation is demonstrated in Figure 7. At the end of the experiments, the SOA estimated from these speciated VOCs accounted for about 25 % and 53 % of the measured SOA formation from the GDI and PFI vehicle exhausts, respectively. Similar to the results of previous studies (Platt et al., 2013; Nordin et al., 2013; Gordon et al., 2014), single-ring aromatics play an important role in the SOA formation, especially for the PFI vehicle which shows higher predicted SOA fraction.

The unpredicted fraction of the measured SOA in the chamber experiments was in the range of 47-75 %. Contributions from IVOCs and semivolatile organic compounds (SVOCs), e.g., long branched and cyclic alkanes and gas-phase polycyclic aromatic hydrocarbons could be a possible explanation for this underestimation. The SOA formed by oxidation of IVOCs and SVOCs is found to dominate over that from single-ring aromatics (Robinson et al., 2007; Zhao et al., 2016). The unpredicted SOA ratio exhibited a maximum value at the beginning of the experiment, indicating that the IVOCs and SVOCs with low volatilities produced SOA much more efficiently than the single-ring aromatics with high volatilities, as the first generation products of photo-oxidation of these precursors form SOA (Robinson et al., 2007).

The larger fraction of the unpredicted SOA from the GDI vehicle exhaust might be associated with higher IVOCs and SVOCs emissions. Gas-phase PAH is one of the main component of speciated IVOCs (Zhao et al., 2016). The particulate-phase PAHs from the GDI vehicle were more abundant than those from the PFI vehicle by a factor of 1.5 (section 3.1). Based on gas-particle equilibrium, this indicates that more gas-phase PAHs, including some aromatic IVOCs, might be emitted by the GDI vehicles, which contribute to the SOA enhancement.

4 Discussion and conclusions

GDI and PFI vehicles have different fuel injection technologies in their engines, which affects their emissions of gaseous and particulate pollutants. In GDI engine, the fuel is directly injected into cylinder, which benefits the fuel atomization and vaporization and provides better control of fuel volume and the combustion process (Liang et

al. 2013; Gao et al., 2015). Thus, in this study, the tested GDI vehicle has higher fuel economy and lower THC emission than the PFI vehicle. However, the insufficient mixing time allowed for the fuel and air leads to incomplete combustion in the GDI engine (Fu et al., 2014). In addition, direct fuel injection leads to fuel impingement onto surfaces of combustion chamber, where liquid pools form, favoring soot-like particulate formation (Ueberall et al., 2015; Chen et al., 2017). Consequently, larger particle mass and number are emitted by the GDI vehicle than from the PFI vehicle. The particles emitted by the GDI vehicle have higher EC mass fraction, leading to a lower OC/EC ratio. The considerable particle number emitted by gasoline vehicles, especially in GDI vehicles exhaust, makes a significant contribution to particle number concentration as well as seeds for further reactions in the atmosphere, and needs to be controlled in the future emission standards.

Our results show that the GDI vehicle contributes more to both primary and secondary aerosol than the PFI vehicle, and has greater impact on environment and air quality. In recent years, the market share of GDI vehicles exerts a continuous growth in China because they provide better fuel economy and lower CO₂ emissions. In 2016, GDI vehicles accounted for 25 % of China's market share in sales, and this proportion is expected to reach 60 % by 2020 (Wen et al., 2016). The PM enhancement of GDI vehicles with increasing population could potentially offset any PM emission reduction benefits, including the development of gasoline emission and fuel standards and the advanced engine technologies of gasoline vehicles. Therefore, our results highlight the necessity of further research and regulation of GDI vehicles.

It should be pointed out that the SOA formation factors in this study are based on one GDI vehicle and one PFI vehicle. Some previous studies proposed that vehicles have variations even though they meet similar specification vehicles and use the same fuel (Gordon et al., 2014; Jathar et al., 2014). Thus more researches with more vehicles for each technology are needed on SOA formation from vehicle exhaust.

Primary emissions and secondary organic formation from one GDI vehicle and one PFI vehicle were investigated when driving under cold-start BJC. The primary PM emitted by the GDI vehicle was 1.4 times greater than that from the PFI vehicle and the SOA formation from the GDI vehicle exhaust was 2.7 times greater than that from the PFI vehicle exhaust for the same OH exposure. The SOA production factors were 54.77 ± 10.70 mg kg⁻

fuel⁻¹ or 3.06±0.60 mg km⁻¹ for the GDI vehicle and 20.57±5.82 mg kg-fuel⁻¹ or 1.55±0.44 mg km⁻¹ for the PFI vehicle at an OH exposure of 5×10⁶ molecular cm⁻³ h, which is consistent with the values seen in previous studies. Considering the higher amounts of OA derived from primary emission and secondary formation, the GDI vehicle contribute considerably more to particle mass concentrations in the ambient air than the PFI vehicle.

The SOA formation was predicted from the gaseous precursors emitted by the GDI and PFI vehicles under high NO_x condition. Single-ring aromatic VOCs could explain only 25-53 % of the measured SOA formation in the chamber experiments. The GDI vehicle exhibited higher fraction of unexplained SOA. More IVOCs and SVOCs were inferred as being emitted by the GDI vehicle.

With increasing population of GDI vehicles, any benefits of the aerosol emission reduction of gasoline vehicles are substantially offset, because GDI vehicles have significant contributions to ambient aerosols. More work is needed to improve the understanding of GDI vehicle emissions and to provide information for the regulation of gasoline vehicles.

337

338

Data availability. The data presented in this article are available from the authors upon request (minhu@pku.edu.cn).

341

342

343 **Acknowledgments**

This work was supported by the National Basic Research Program of China (973 Program) (2013CB228503, 2013CB228502), National Natural Science Foundation of China (91544214, 41421064, 51636003), the Strategic Priority Research Program of Chinese Academy of Sciences (XDB05010500), China Postdoctoral Science Foundation (2015M580929), and the National Science and Technology Support Program (2014BAC21B01). We also thank the State Key Lab of Automotive Safety and Energy at Tsinghua University for the support to experiments.

351 **Reference**

- 352 Alkidas, A. C.: Combustion advancements in gasoline engines, *Energy Conversion and Management*, 48, 2751-
353 2761, 10.1016/j.enconman.2007.07.027, 2007.
- 354 Bahreini, R., Middlebrook, A. M., de Gouw, J. A., Warneke, C., Trainer, M., Brock, C. A., Stark, H., Brown, S. S.,
355 Dube, W. P., Gilman, J. B., Hall, K., Holloway, J. S., Kuster, W. C., Perring, A. E., Prevot, A. S. H., Schwarz, J. P.,
356 Spackman, J. R., Szidat, S., Wagner, N. L., Weber, R. J., Zotter, P., and Parrish, D. D.: Gasoline emissions dominate
357 over diesel in formation of secondary organic aerosol mass, *Geophysical Research Letters*, 39,
358 10.1029/2011gl050718, 2012.
- 359 Chen, L., Liang, Z., Zhang, X., and Shuai, S.: Characterizing particulate matter emissions from GDI and PFI
360 vehicles under transient and cold start conditions, *Fuel*, 189, 131-140, 10.1016/j.fuel.2016.10.055, 2017.
- 361 DeCarlo, P. F., Kimmel, J. R., Trimborn, A., Northway, M. J., Jayne, J. T., Aiken, A. C., Gonin, M., Fuhrer, K.,
362 Horvath, T., Docherty, K. S., Worsnop, D. R., and Jimenez, J. L.: Field-deployable, high-resolution, time-of-flight
363 aerosol mass spectrometer, *Analytical Chemistry*, 78, 8281-8289, 10.1021/ac061249n, 2006.
- 364 Donahue, N. M., Robinson, A. L., Stanier, C. O., and Pandis, S. N.: Coupled partitioning, dilution, and chemical
365 aging of semivolatile organics, *Environ. Sci. Technol.*, 40, 2635-2643, 10.1021/es052297c, 2006.
- 366 Du, Z., Hu, M., Peng, J., Guo, S., Zheng, R., Zheng, J., Shang, D., Qin, Y., Niu, H., Li, M., Yang, Y., Lu, S., Wu,
367 Y., Shao, M., and Shuai, S.: Potential of secondary aerosol formation from Chinese gasoline engine exhaust, *Journal*
368 *of environmental sciences (China)*, 66, 348-357, 10.1016/j.jes.2017.02.022, 2018.
- 369 Fu, H., Wang, Y., Li, X., and Shuai, S.: Impacts of Cold-Start and Gasoline RON on Particulate Emission from
370 Vehicles Powered by GDI and PFI Engines, *SAE Technical Paper*, 2014-01-2836, 10.4271/2014-01-2836, 2014.
- 371 Gao, Z., Curran, S. J., Parks, J. E., II, Smith, D. E., Wagner, R. M., Daw, C. S., Edwards, K. D., and Thomas, J. F.:
372 Drive cycle simulation of high efficiency combustions on fuel economy and exhaust properties in light-duty
373 vehicles, *Applied Energy*, 157, 762-776, 10.1016/j.apenergy.2015.03.070, 2015.
- 374 Gentner, D. R., Jathar, S. H., Gordon, T. D., Bahreini, R., Day, D. A., El Haddad, I., Hayes, P. L., Pieber, S. M.,
375 Platt, S. M., de Gouw, J., Goldstein, A. H., Harley, R. A., Jimenez, J. L., Prevot, A. S. H., and Robinson, A. L.:

376 Review of Urban Secondary Organic Aerosol Formation from Gasoline and Diesel Motor Vehicle Emissions,
 377 Environmental science & technology, 51, 1074-1093, 10.1021/acs.est.6b04509, 2017.

378 Gordon, T. D., Presto, A. A., May, A. A., Nguyen, N. T., Lipsky, E. M., Donahue, N. M., Gutierrez, A., Zhang, M.,
 379 Maddox, C., Rieger, P., Chattopadhyay, S., Maldonado, H., Maricq, M. M., and Robinson, A. L.: Secondary organic
 380 aerosol formation exceeds primary particulate matter emissions for light-duty gasoline vehicles, Atmos. Chem.
 381 Phys. , 14, 4661-4678, 10.5194/acp-14-4661-2014, 2014.

382 Guo, S., Hu, M., Zamora, M. L., Peng, J., Shang, D., Zheng, J., Du, Z., Wu, Z., Shao, M., Zeng, L., Molina, M. J.,
 383 and Zhang, R.: Elucidating severe urban haze formation in China, Proceedings of the National Academy of
 384 Sciences of the United States of America, 111, 17373-17378, 10.1073/pnas.1419604111, 2014.

385 Hayes, P. L., Ortega, A. M., Cubison, M. J., Froyd, K. D., Zhao, Y., Cliff, S. S., Hu, W. W., Toohey, D. W., Flynn,
 386 J. H., Lefer, B. L., Grossberg, N., Alvarez, S., Rappenglueck, B., Taylor, J. W., Allan, J. D., Holloway, J. S., Gilman,
 387 J. B., Kuster, W. C., De Gouw, J. A., Massoli, P., Zhang, X., Liu, J., Weber, R. J., Corrigan, A. L., Russell, L. M.,
 388 Isaacman, G., Worton, D. R., Kreisberg, N. M., Goldstein, A. H., Thalman, R., Waxman, E. M., Volkamer, R., Lin,
 389 Y. H., Surratt, J. D., Kleindienst, T. E., Offenberg, J. H., Dusanter, S., Griffith, S., Stevens, P. S., Brioude, J.,
 390 Angevine, W. M., and Jimenez, J. L.: Organic aerosol composition and sources in Pasadena, California, during the
 391 2010 CalNex campaign, Journal of Geophysical Research-Atmospheres, 118, 9233-9257, 10.1002/jgrd.50530,
 392 2013.

393 Hays, M. D., Preston, W., George, B. J., Schmid, J., Baldauf, R., Snow, R., Robinson, J. R., Long, T., and Faircloth,
 394 J.: Carbonaceous aerosols emitted from light-duty vehicles operating on gasoline and ethanol fuel blends,
 395 Environmental science & technology, 47, 14502-14509, 10.1021/es403096v, 2013.

396 Hu, W., Hu, M., Hu, W., Jimenez, J. L., Yuan, B., Chen, W., Wang, M., Wu, Y., Chen, C., Wang, Z., Peng, J., Zeng,
 397 L., and Shao, M.: Chemical composition, sources, and aging process of submicron aerosols in Beijing: Contrast
 398 between summer and winter, Journal of Geophysical Research-Atmospheres, 121, 1955-1977,
 399 10.1002/2015jd024020, 2016.

400 Huang, R.-J., Zhang, Y., Bozzetti, C., Ho, K.-F., Cao, J.-J., Han, Y., Daellenbach, K. R., Slowik, J. G., Platt, S. M.,
 401 Canonaco, F., Zotter, P., Wolf, R., Pieber, S. M., Bruns, E. A., Crippa, M., Ciarelli, G., Piazzalunga, A.,
 402 Schwikowski, M., Abbaszade, G., Schnelle-Kreis, J., Zimmermann, R., An, Z., Szidat, S., Baltensperger, U.,
 403 Haddad, I. E., and Prévôt, A. S. H.: High secondary aerosol contribution to particulate pollution during haze events
 404 in China, *Nature*, 10.1038/nature13774, 2014.

405 Ito, Y., Shimoda, T., Aoki, T., Yuuki, K., Sakamoto, H., Kato, K., Their, D., Kattouah, P., Ohara, E. and Vogt, C.:
 406 Next Generation of Ceramic Wall Flow Gasoline Particulate Filter with Integrated Three Way Catalyst, SAE
 407 Technical Paper 2015-01-1073, 2015, doi:10.4271/2015-01-1073, 2015.

408 Jathar, S. H., Gordon, T. D., Hennigan, C. J., Pye, H. O. T., Pouliot, G., Adams, P. J., Donahue, N. M., and Robinson,
 409 A. L.: Unspeciated organic emissions from combustion sources and their influence on the secondary organic aerosol
 410 budget in the United States, *Proc. Natl. Acad. Sci. USA*, 111, 10473-10478, 10.1073/pnas.1323740111, 2014.

411 Jathar, S. H., Woody, M., Pye, H. O. T., Baker, K. R., and Robinson, A. L.: Chemical transport model simulations
 412 of organic aerosol in southern California: model evaluation and gasoline and diesel source contributions,
 413 *Atmospheric Chemistry and Physics*, 17, 4305-4318, 10.5194/acp-17-4305-2017, 2017.

414 Kamal, A., Cincinelli, A., Martellini, T., and Malik, R. N.: A review of PAH exposure from the combustion of
 415 biomass fuel and their less surveyed effect on the blood parameters, *Environmental Science and Pollution Research*,
 416 22, 4076-4098, 10.1007/s11356-014-3748-0, 2015.

417 Kanakidou, M., Seinfeld, J. H., Pandis, S. N., Barnes, I., Dentener, F. J., Facchini, M. C., Van Dingenen, R., Ervens,
 418 B., Nenes, A., Nielsen, C. J., Swietlicki, E., Putaud, J. P., Balkanski, Y., Fuzzi, S., Horth, J., Moortgat, G. K.,
 419 Winterhalter, R., Myhre, C. E. L., Tsigaridis, K., Vignati, E., Stephanou, E. G., and Wilson, J.: Organic aerosol and
 420 global climate modelling: a review, *Atmospheric Chemistry and Physics*, 5, 1053-1123, 2005.

421 Kramp, F., and Paulson, S. E.: On the uncertainties in the rate coefficients for OH reactions with hydrocarbons, and
 422 the rate coefficients of the 1,3,5-trimethylbenzene and m-xylene reactions with OH radicals in the gas phase,
 423 *Journal of Physical Chemistry A*, 102, 2685-2690, 10.1021/jp973289o, 1998.

424 Li, M., Hu, M., Wu, Y., Qin, Y., Zheng, R., Peng, J., Guo, Q., Xiao, Y., Hu, W., Zheng, J., Du, Z., Xiao, J., Shuai,
 425 S.: Characteristics of Particulate Organic Matters Emissions from Gasoline Direct Injection Engine and Its
 426 Influence Factors, *Proceedings of the Chinese Society of Electrical Engineering*, 36, 4443-4451.
 427 Liang, B., Ge, Y., Tan, J., Han, X., Gao, L., Hao, L., Ye, W., and Dai, P.: Comparison of PM emissions from a
 428 gasoline direct injected (GDI) vehicle and a port fuel injected (PFI) vehicle measured by electrical low pressure
 429 impactor (ELPI) with two fuels: Gasoline and M15 methanol gasoline, *Journal of Aerosol Science*, 57, 22-31,
 430 10.1016/j.jaerosci.2012.11.008, 2013.
 431 Lindinger, W., Hansel, A., and Jordan, A.: On-line monitoring of volatile organic compounds at pptv levels by
 432 means of proton-transfer-reaction mass spectrometry (PTR-MS) - Medical applications, food control and
 433 environmental research, *International Journal of Mass Spectrometry*, 173, 191-241, 10.1016/s0168-
 434 1176(97)00281-4, 1998.
 435 Liu, T., Wang, X., Deng, W., Hu, Q., Ding, X., Zhang, Y., He, Q., Zhang, Z., Lü S., Bi, X., Chen, J., and Yu, J.:
 436 Secondary organic aerosol formation from photochemical aging of light-duty gasoline vehicle exhausts in a smog
 437 chamber, *Atmos. Chem. Phys.*, 15, 9049-9062, 10.5194/acp-15-9049-2015, 2015.
 438 Lu, K. D., Hofzumahaus, A., Holland, F., Bohn, B., Brauers, T., Fuchs, H., Hu, M., Häeler, R., Kita, K., Kondo,
 439 Y., Li, X., Lou, S. R., Oebel, A., Shao, M., Zeng, L. M., Wahner, A., Zhu, T., Zhang, Y. H., and Rohrer, F.: Missing
 440 OH source in a suburban environment near Beijing: observed and modelled OH and HO₂
 441 concentrations in summer 2006, *Atmos. Chem. Phys.*, 13, 1057-1080, 10.5194/acp-13-1057-2013, 2013.
 442 Maria, S. F., Russell, L. M., Gilles, M. K., and Myneni, S. C. B.: Organic aerosol growth mechanisms and their
 443 climate-forcing implications, *Science*, 306, 1921-1924, 10.1126/science.1103491, 2004.
 444 Maricq, M. M., Podsiadlik, D. H., and Chase, R. E.: Gasoline vehicle particle size distributions: Comparison of
 445 steady state, FTP, and US06 measurements, *Environmental science & technology*, 33, 2007-2015,
 446 10.1021/es981005n, 1999.

Mathis, U., Mohr, M., and Forss, A. M.: Comprehensive particle characterization of modern gasoline and diesel passenger cars at low ambient temperatures, *Atmospheric Environment*, 39, 107-117, 10.1016/j.atmosenv.2004.09.029, 2005.

May, A. A., Nguyen, N. T., Presto, A. A., Gordon, T. D., Lipsky, E. M., Karve, M., Gutierrez, A., Robertson, W. H., Zhang, M., Brandow, C., Chang, O., Chen, S., Cicero-Fernandez, P., Dinkins, L., Fuentes, M., Huang, S.-M., Ling, R., Long, J., Maddox, C., Massetti, J., McCauley, E., Miguel, A., Na, K., Ong, R., Pang, Y., Rieger, P., Sax, T., Tin, T., Thu, V., Chattopadhyay, S., Maldonado, H., Maricq, M. M., and Robinson, A. L.: Gas- and particle-phase primary emissions from in-use, on-road gasoline and diesel vehicles, *Atmospheric Environment*, 88, 247-260, 10.1016/j.atmosenv.2014.01.046, 2014.

Myung, C.-L., Kim, J., Choi, K., Hwang, I. G., and Park, S.: Comparative study of engine control strategies for particulate emissions from direct injection light-duty vehicle fueled with gasoline and liquid phase liquefied petroleum gas (LPG), *Fuel*, 94, 348-355, 10.1016/j.fuel.2011.10.041, 2012.

Ng, N. L., Kroll, J. H., Chan, A. W. H., Chhabra, P. S., Flagan, R. C., and Seinfeld, J. H.: Secondary organic aerosol formation from m-xylene, toluene, and benzene, *Atmos. Chem. Phys.*, 7, 3909–3922, 2007.

Nordin, E. Z., Eriksson, A. C., Roldin, P., Nilsson, P. T., Carlsson, J. E., Kajos, M. K., Hellén, H., Wittbom, C., Rissler, J., Löndahl, J., Swietlicki, E., Svenningsson, B., Bohgard, M., Kulmala, M., Hallquist, M., and Pagels, J. H.: Secondary organic aerosol formation from idling gasoline passenger vehicle emissions investigated in a smog chamber, *Atmos. Chem. Phys.*, 13, 6101-6116, 10.5194/acp-13-6101-2013, 2013.

Odum, J. R., Hoffmann, T., Bowman, F., Collins, D., Flagan, R. C., and Seinfeld, J. H.: Gas/particle partitioning and secondary organic aerosol yields, *Environ. Sci. Technol.*, 30, 2580-2585, 10.1021/es950943+, 1996.

Peng, J., Hu, M., Du, Z., Wang, Y., Zheng, J., Zhang, W., Yang, Y., Qin, Y., Zheng, R., Xiao, Y., Wu, Y., Lu, S., Wu, Z., Guo, S., Mao, H., and Shuai, S.: Gasoline aromatic: a critical determinant of urban secondary organic aerosol formation, *Atmospheric Chemistry and Physics*, 2017, in press.

Platt, S. M., El Haddad, I., Zardini, A. A., Clairotte, M., Astorga, C., Wolf, R., Slowik, J. G., Temime-Roussel, B., Marchand, N., Ježek, I., Drinovec, L., Močnik, G., Möhler, O., Richter, R., Barmet, P., Bianchi, F., Baltensperger,

U., and Prévôt, A. S. H.: Secondary organic aerosol formation from gasoline vehicle emissions in a new mobile environmental reaction chamber, *Atmos. Chem. Phys.*, 13, 9141-9158, 10.5194/acp-13-9141-2013, 2013.

Robinson, A. L., Donahue, N. M., Shrivastava, M. K., Weitkamp, E. A., Sage, A. M., Grieshop, A. P., Lane, T. E., Pierce, J. R., and Pandis, S. N.: Rethinking organic aerosols: Semivolatile emissions and photochemical aging, *Science*, 315, 1259-1262, 10.1126/science.1133061, 2007.

Saliba, G., Saleh, R., Zhao, Y., Presto, A. A., Lambe, A. T., Frodin, B., Sardar, S., Maldonado, H., Maddox, C., May, A. A., Drozd, G. T., Goldstein, A. H., Russell, L. M., Hagen, F., and Robinson, A. L.: Comparison of Gasoline Direct-Injection (GDI) and Port Fuel Injection (PFI) Vehicle Emissions: Emission Certification Standards, Cold-Start, Secondary Organic Aerosol Formation Potential, and Potential Climate Impacts, *Environmental science & technology*, 51, 6542-6552, 10.1021/acs.est.6b06509, 2017.

Schauer, J. J., Kleeman, M. J., Cass, G. R. and Simoneit, B. R. T.: Measurement of Emissions from Air Pollution Sources. 5. C1-C32 Organic Compounds from Gasoline-Powered Motor Vehicles, *Environmental science & technology*, 36, 1169-1180, 2002.

Seinfeld, J. H., Kleindienst, T. E., Edney, E. O., and Cohen, J. B.: Aerosol growth in a steady-state, continuous flow chamber: Application to studies of secondary aerosol formation, *Aerosol Science and Technology*, 37, 728-734, 10.1080/02786820390214954, 2003.

Song, C., Na, K. S., and Cocker, D. R.: Impact of the hydrocarbon to NO_x ratio on secondary organic aerosol formation, *Environ. Sci. Technol.*, 39, 3143-3149, 10.1021/es0493244, 2005.

Ueberall, A., Otte, R., Eilts, P., and Krahel, J.: A literature research about particle emissions from engines with direct gasoline injection and the potential to reduce these emissions, *Fuel*, 147, 203-207, 10.1016/j.fuel.2015.01.012, 2015.

Wang, Y., Zheng, R., Qin, Y., Peng, J., Li, M., Lei, J., Wu, Y., Hu, M., and Shuai, S.: The impact of fuel compositions on the particulate emissions of direct injection gasoline engine, *Fuel*, 166, 543-552, 10.1016/j.fuel.2015.11.019, 2016.

496 Wang, Z. B., Hu, M., Wu, Z. J., Yue, D. L., He, L. Y., Huang, X. F., Liu, X. G., and Wiedensohler, A.: Long-term
 497 measurements of particle number size distributions and the relationships with air mass history and source
 498 apportionment in the summer of Beijing, *Atmospheric Chemistry and Physics*, 13, 10159-10170, 10.5194/acp-13-
 499 10159-2013, 2013.

500 Wen, Y., Wang, Y., Fu, C., Deng, W., Zhan, Z., Tang, Y., Li, X., Ding, H., and Shuai, S.: The Impact of Injector
 501 Deposits on Spray and Particulate Emission of Advanced Gasoline Direct Injection Vehicle, *SAE Technical Paper*,
 502 2016-01-2284, 10.4271/2016-01-2284, 2016.

503 Yang, B., Ma, P. K., Shu, J. N., Zhang, P., Huang, J. Y. and Zhang, H. X.: Formation mechanism of secondary
 504 organic aerosol from ozonolysis of gasoline vehicle exhaust, *Environmental Pollution*, 234, 960-968,
 505 10.1016/j.envpol.2017.12.048, 2018.

506 Yuan, B., Shao, M., de Gouw, J., Parrish, D. D., Lu, S., Wang, M., Zeng, L., Zhang, Q., Song, Y., Zhang, J., and
 507 Hu, M.: Volatile organic compounds (VOCs) in urban air: How chemistry affects the interpretation of positive
 508 matrix factorization (PMF) analysis, *Journal of Geophysical Research: Atmospheres*, 117, n/a-n/a,
 509 10.1029/2012jd018236, 2012.

510 Zhang, Q., Jimenez, J. L., Canagaratna, M. R., Allan, J. D., Coe, H., Ulbrich, I., Alfarra, M. R., Takami, A.,
 511 Middlebrook, A. M., Sun, Y. L., Dzepina, K., Dunlea, E., Docherty, K., DeCarlo, P. F., Salcedo, D., Onasch, T.,
 512 Jayne, J. T., Miyoshi, T., Shimon, A., Hatakeyama, S., Takegawa, N., Kondo, Y., Schneider, J., Drewnick, F.,
 513 Borrmann, S., Weimer, S., Demerjian, K., Williams, P., Bower, K., Bahreini, R., Cottrell, L., Griffin, R. J.,
 514 Rautiainen, J., Sun, J. Y., Zhang, Y. M., and Worsnop, D. R.: Ubiquity and dominance of oxygenated species in
 515 organic aerosols in anthropogenically-influenced Northern Hemisphere midlatitudes, *Geophysical Research Letters*,
 516 34, 10.1029/2007gl029979, 2007.

517 Zhang, X., Cappa, C. D., Jathar, S. H., McVay, R. C., Ensberg, J. J., Kleeman, M. J., and Seinfeld, J. H.: Influence
 518 of vapor wall loss in laboratory chambers on yields of secondary organic aerosol, *Proc. Natl. Acad. Sci. USA*, 111,
 519 5802-5807, 10.1073/pnas.1404727111, 2014.

520 Zhao, B., Wang, S., Donahue, N. M., Jathar, S. H., Huang, X., Wu, W., Hao, J., and Robinson, A. L.: Quantifying
521 the effect of organic aerosol aging and intermediate-volatility emissions on regional-scale aerosol pollution in
522 China, *Scientific Reports*, 6, 10.1038/srep28815, 2016.

523 Zhao, Y., Nguyen, N. T., Presto, A. A., Hennigan, C. J., May, A. A., and Robinson, A. L.: Intermediate Volatility
524 Organic Compound Emissions from On-Road Gasoline Vehicles and Small Off-Road Gasoline Engines,
525 *Environmental science & technology*, 50, 4554-4563, 10.1021/acs.est.5b06247, 2016.

526 Zhao, Y., Saleh, R., Saliba, G., Presto, A. A., Gordon, T. D., Drozd, G. T., Goldstein, A. H., Donahue, N. M., and
527 Robinson, A. L.: Reducing secondary organic aerosol formation from gasoline vehicle exhaust, *Proceedings of the*
528 *National Academy of Sciences of the United States of America*, 114, 6984-6989, 10.1073/pnas.1620911114, 2017.

529 Zhu, R., Hu, J., Bao, X., He, L., Lai, Y., Zu, L., Li, Y., and Su, S.: Tailpipe emissions from gasoline direct injection
530 (GDI) and port fuel injection (PFI) vehicles at both low and high ambient temperatures, *Environmental Pollution*,
531 216, 223-234, 10.1016/j.envpol.2016.05.066, 2016.

532 Zimmerman, N., Wang, J. M., Jeong, C.-H., Ramos, M., Hilker, N., Healy, R. M., Sabaliauskas, K., Wallace, J. S.,
533 and Evans, G. J.: Field Measurements of Gasoline Direct Injection Emission Factors: Spatial and Seasonal
534 Variability, *Environmental science & technology*, 50, 2035-2043, 10.1021/acs.est.5b04444, 2016.

535

536 Table 1 Descriptions of the gasoline direct injection (GDI) and port fuel injection (PFI) vehicles used in the
537 experiments.

| Vehicle | Make and model | Emission standard class | Model year | Mileage (km) | Displacement (cm ³) | Power (kW) | Weight (kg) |
|---------|-------------------|----------------------------|---------------|-----------------|------------------------------------|---------------|----------------|
| GDI | VW Sagitar | China V | 2015 | 3000 | 1395 | 110 | 1395 |
| PFI | Honda Civic | China IV | 2009 | 42500 | 1799 | 103 | 1280 |

538

539 Table 2 Overview of all instruments used to measure the gas and particulate phase pollutants in the experiments.

| Parameter | Phase | Instrument | Note |
|---|----------|--|----------|
| CO, CO ₂ , NO _x and total hydrocarbon (THC) concentration | Gas | Gas analyzer AVL Combustion Emissions Bench II | On-line |
| Aerosol number size distribution | Particle | DMS500 | On-line |
| PM _{2.5} | Particle | Balance (AX105DR) | Off-line |
| Organic carbon/Elemental carbon concentration | Particle | OC/EC analyzer | Off-line |
| CO concentration | Gas | 48i CO analyzer | On-line |
| NO, NO ₂ , and NO _x concentration | Gas | 42i NO-NO ₂ -NO _x analyzer | On-line |
| O ₃ concentration | Gas | 49i O ₃ analyzer | On-line |
| VOCs concentration | Gas | Proton transfer reaction mass spectrometer (PTR-MS) | On-line |
| Aerosol number (mass) size distribution | Particle | Scanning mobility particle sizer (SMPS, consist of 3081-DMA and 3775-CPC), | On-line |
| Size resolved non-refractory aerosol | Particle | High resolution time-of-flight aerosol mass spectrometer (HR-Tof-AMS) | On-line |

540

541

542

Table 3 Emission factors (EFs) of gaseous pollutants from the gasoline direct injection (GDI) and port fuel injection (PFI) vehicles in

543

this study and those of previous studies.

| | This study | | | | Saliba et al., 2017 | | May et al., 2014 | Platt et al., 2013 | | Zhu et al., 2016 | |
|-----------------|-----------------------------|--------------------|-----------------------------|--------------------|----------------------|--------------------|-------------------------|-------------------------|--------------------|------------------------|--------------------|
| | GDI | | PFI | | GDI | PFI | PFI ^a | | | GDI | PFI |
| | China V | | China IV | | ULEV | ULEV | LEV II | Euro V | | China IV | China IV |
| | Cold BJC | | | | Cold UC ^b | | Cold UC | Cold NEDC | | Cold WLTC ^c | |
| | g kg- fuel ⁻¹ | g km ⁻¹ | g kg- fuel ⁻¹ | g km ⁻¹ | g km ⁻¹ | g km ⁻¹ | g kg-fuel ⁻¹ | g kg-fuel ⁻¹ | g km ⁻¹ | g km ⁻¹ | g km ⁻¹ |
| CO ₂ | 3439 | 213 | 3350 | 283 | - | - | - | - | - | 187 | 215 |
| | ±23 | ±4 | ±24 | ±4 | | | | | | | |
| THC | 1.55 | 0.09 | 1.70 | 0.13 | 0.02 | 0.06 | 0.64 | 0.91-1.06 | 0.036- | 0.05 | 0.03 |
| | ±0.22 | ±0.01 | ±0.19 | ±0.01 | | | | | 0.042 | | |
| Benzene | 0.056 | 0.003 | 0.061 | 0.005 | - | - | 0.018 | - | 0.002 | - | - |
| | ±0.011 | ±0.001 | ±0.016 | ±0.001 | | | | | | | |
| Toluene | 0.101 | 0.006 | 0.220 | 0.017 | - | - | 0.026 | - | 0.002 | - | - |
| | ±0.004 | ±0.001 | ±0.047 | ±0.004 | | | | | | | |

544

^a 22 PFI vehicles and 3 GDI vehicles;

545

^b UC: Unified Cycle;

546

^c WLTC: Worldwide-harmonized Light-duty Test Cycle

547 Table 4 EFs of primary aerosols, including carbonaceous aerosols and particulate polycyclic aromatic hydrocarbons (PAHs) from the
548 GDI and PFI vehicles in this study and those of previous studies.

| | This study | | | | Saliba et al., 2017 | | May et al., 2014 | Platt et al., 2013 | | Zhu et al., 2016 | |
|-------------------------|--------------------|---------------------|--------------------|---------------------|---------------------|---------------------|--------------------------|--------------------|---------------------|---------------------|---------------------|
| | GDI | | PFI | | GDI | PFI | PFI | | | GDI | PFI |
| | China V | | China IV | | ULEV | ULEV | LEV II | Euro V | | China IV | China IV |
| | Cold BJC | | | | Cold UC | | Cold UC | Cold NEDC | | Cold WLTC | |
| | mg kg- | mg km ⁻¹ | mg kg- | mg km ⁻¹ | mg km ⁻¹ | mg km ⁻¹ | mg kg-fuel ⁻¹ | mg kg- | mg km ⁻¹ | mg km ⁻¹ | mg km ⁻¹ |
| | fuel ⁻¹ | | fuel ⁻¹ | | | | | fuel ⁻¹ | | | |
| PM _{2.5} | 61.7±24.5 | 3.4±1.4 | 33.4±25.6 | 2.5±1.9 | 3.9 | 2.4 | 18.0 | - | - | 1.5 | 1.0 |
| EC | 10.7±3.6 | 0.6±0.2 | 2.4±1.6 | 0.2±0.1 | 3.0 | 0.6 | 12.2 | 11.2-20.0 | 1.2-1.7 | - | - |
| POA | 41.7±9.8 | 2.3±0.6 | 25.0±0.3 | 1.9±0.1 | 0.4 | 0.6 | 5.2 | 24.5-19.7 | 0.4-1.4 | - | - |
| OC/EC | 3.2 | | 8.7 | | 0.1 | 0.8 | 0.4 | 0.2-1.8 | | - | - |
| PAHs(×10 ⁶) | 20.4±2.1 | 1.1±0.1 | 13.2±4.1 | 1.0±0.3 | - | - | - | - | - | - | - |

549
550

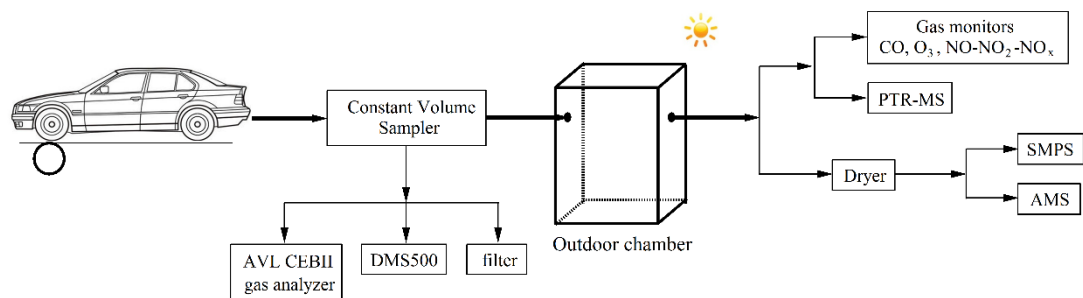
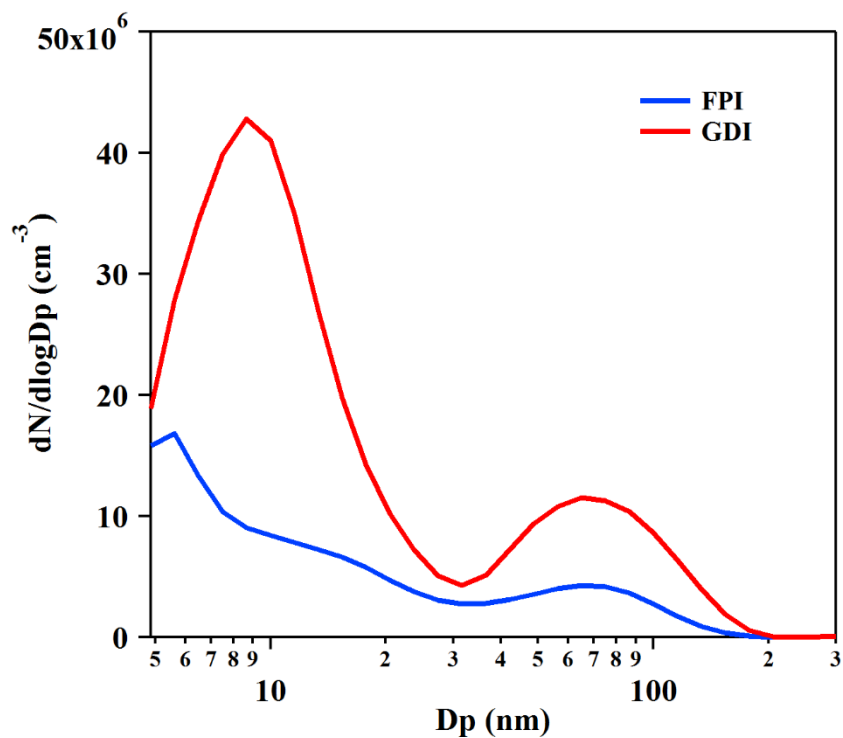


Figure 1. Schematic diagram of the outdoor chamber set up for the experiments.



554
 555 Figure 2. Number size distributions of primary PM emitted from the GDI (red line) and PFI (blue line) gasoline
 556 vehicles. The results are average of particle number emissions from vehicles during a whole BJC, measured by
 557 DMS500 in the CVS system. The particles were heated to 150°C in the DMS500.
 558

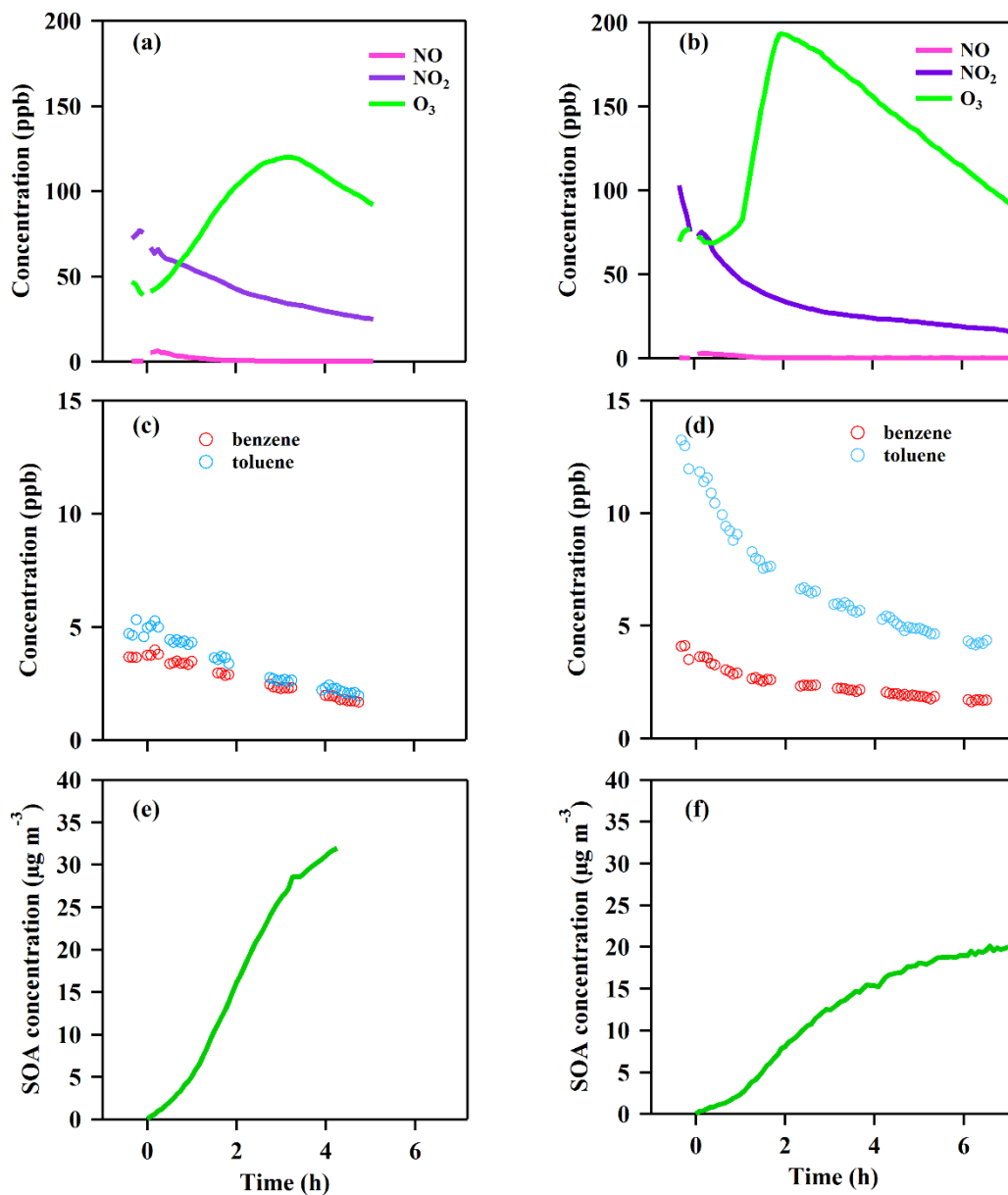
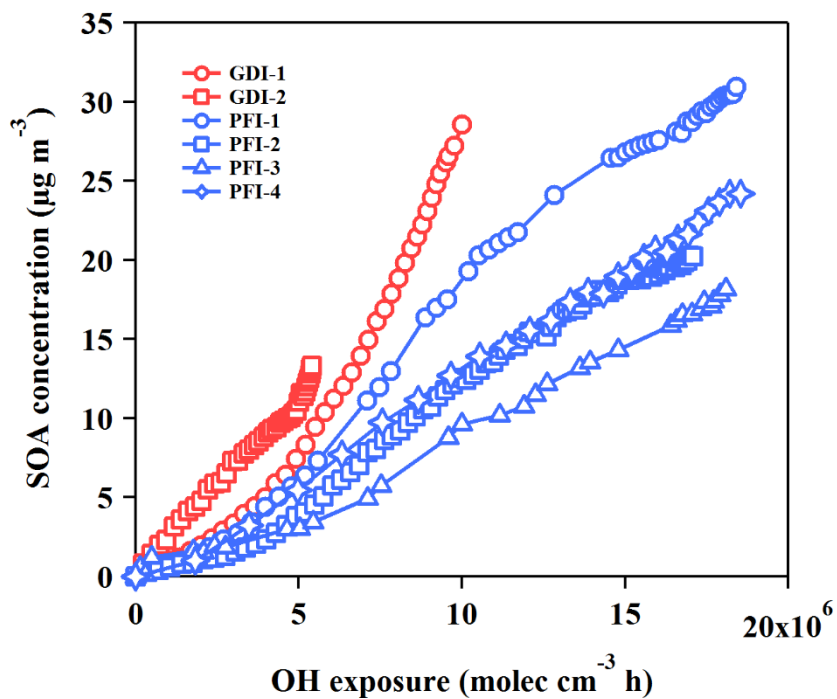


Figure 3. Time series of the gases and particle evolutions over the photochemical age in the chamber experiments from the GDI vehicle exhaust (a, c, e) and PFI vehicle exhaust (b, d, f). (a, b): NO, NO₂ and O₃ concentration; (c, d): benzene and toluene concentration; (e, f): corrected SOA concentration.

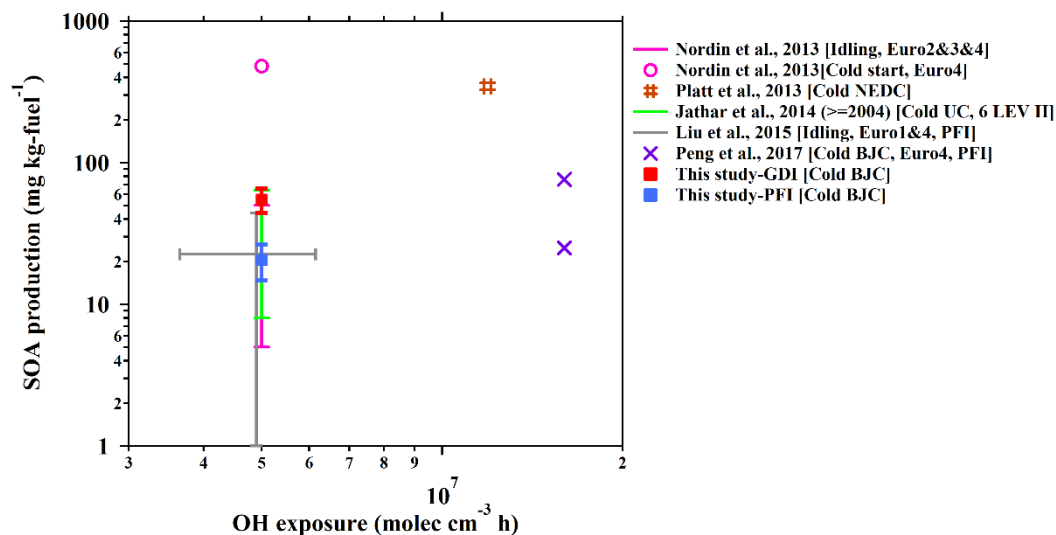


564

565 Figure 4. SOA productions from the GDI vehicle exhaust (red markers) and the PFI vehicle exhaust (blue markers)

566 as functions of OH exposure in the chamber experiments.

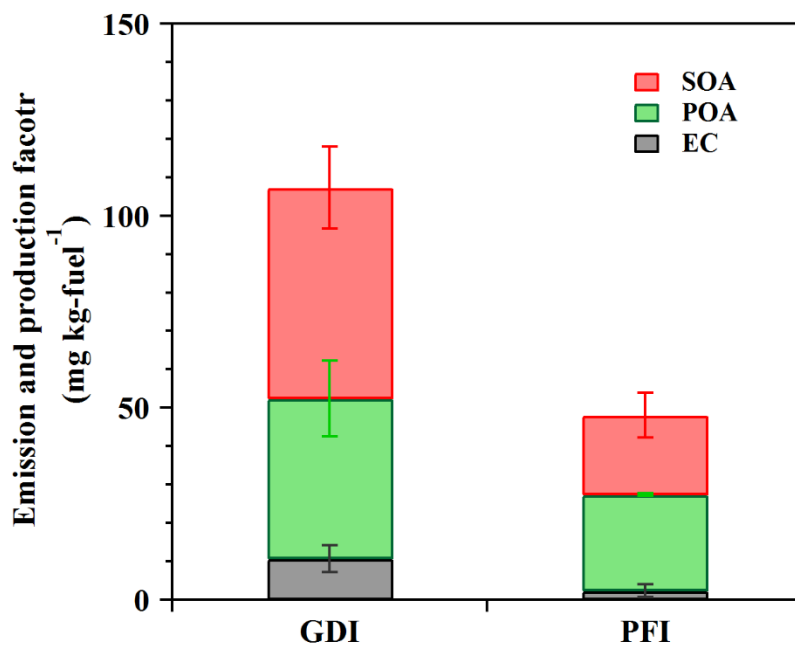
567



568

569 Figure 5. Fuel-based SOA production from gasoline vehicle exhaust as a function of OH exposure in the chamber
 570 simulations. The SOA production data are from published studies of chamber simulation of gasoline vehicle
 571 exhaust. From the study of Jathar et al. (2014), the SOA production of vehicles manufactured in 2004 or later (LEV
 572 II) is selected, which is a model year that is more close to those of the vehicles in this study. The error bars of
 573 previous results indicate the range of OH exposure (x axis) and SOA production (y axis) in their simulations. The
 574 driving cycles and vehicle information are also noted in the legend of each study.

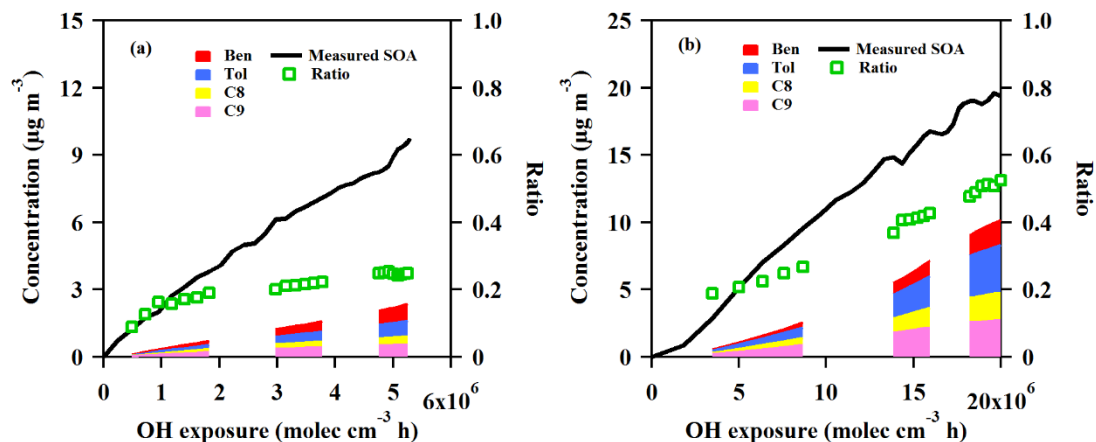
575



576

577 Figure 6 EC and POA EFs as well as corrected SOA production factors from the GDI and PFI vehicle exhausts in
 578 this study (OH exposure = 5×10^6 molecular cm^{-3} h).

579



580

581 Figure 7. Measured and predicted SOA concentration as a function of OH exposure from GDI vehicle exhaust (a)
 582 and PFI vehicle exhaust (b) in the chamber experiments. The black line is the measured SOA concentration with
 583 wall-loss and particle dilution correction during the experiment. The red, blue, yellow and pink areas are predicted
 584 SOA concentration estimated from benzene, toluene, C8 alkylbenzene and C9 alkylbenzene, respectively. The
 585 green markers are the ratios of the predicted SOA to the measured SOA.

586